# Quantifying the auto-oscillation complexity following water spraying with interest for phonation

A. Van Hirtum,* A. Bouvet, and X. Pelorson
*LEGI, UMR CNRS 5519, Grenoble Alpes University, Grenoble, France*

(Received 7 March 2019; revised manuscript received 2 June 2019; published 21 October 2019)

Human voiced sound production or phonation is the result of a fluid-structure instability in the larynx leading to vocal folds auto-oscillation. In this paper, the effect of surface hydration following water spraying (0 up to 5 ml) on an ongoing auto-oscillation is studied experimentally using different mechanical deformable vocal folds replicas. The complexity of the oscillation is quantified on the upstream pressure by a phase space recurrence and complexity analysis. It is shown that: (1) the ratio of the degree of determinism to the recurrence rate of the phase space states $\gamma$ and (2) estimated correlation dimension $D_2$ are suitable parameters to grasp the effect of hydration on the oscillation pattern. The oscillation regime after hydration can either remain deterministic or approach a chaotic regime depending on initial conditions prior to water spraying, such as elasticity, glottal aperture, as well as oscillation complexity.

DOI: 10.1103/PhysRevE.100.043111

## I. INTRODUCTION

Vocal fold (VF) auto-oscillation due to a fluid-structure (FS) instability within the larynx, between airflow coming from the lungs and enveloping VF tissues, provides the main sound source for voiced speech utterances. Observations on human speakers indicate that surface hydration affects the underlying FS interaction and resulting sound properties [1–6]. Whereas the physical principles of the FS instability are well studied [7–9], the physical role of surface hydration for voice production is only marginally investigated [10]. The effect of surface hydration following water spraying with 0 up to 5 ml which is pertinent to artificial sprays used for hydration remediation [11] on an auto-oscillating mechanical VF replica was systematically studied by measuring the upstream pressure [12,13]. Hydration affected the mean as well as fluctuating flow fields during a single oscillation cycle [12]. The mean flow regime shifted from air dominated during the closing phase to air-water mixed flow during the opening phase and the fluctuating flow field exhibited droplet induced turbulence. Changes to the mean flow field explain observed alterations to primary oscillation properties, such as the harmonic properties whereas changes to the fluctuating flow field affect the signal-to-noise ratio and rapid cycle-to-cycle perturbation measures [13]. Mentioned features are commonly assessed when analyzing normal as well as pathological voice signals [1–6]. Additionally, turbulence generation as well as the change in flow regime following water spraying might affect the FS interaction's complexity. Therefore, in this paper, it is aimed to quantify the influence of water spraying on the complexity of the FS instability by considering the correlation dimension estimated from a recurrence analysis of the phase space trajectories. Correlation dimension $D_2$ allows to describe the needed degrees of freedom, i.e., the complexity, with a single parameter, which is not the case when quantifying classic voice signal features. $D_2$ has been used in turbulence studies since the groundbreaking paper by Takens [14] and introduced in human voice analysis studies [15–21]. So far, its use in voice analysis studies is mainly motivated by the development of speech synthesis and recognition technologies where speech is considered as a low-dimensional nonlinear model [10,22,23]. Nevertheless, $D_2$ is also of interest from an aerodynamic point of view in order to further assess the assumption that turbulence, such as the described droplet induced turbulence following water spraying [12], affects not only fricative speech sound production, but might affect voicing as well [24]. Different mechanical VF replicas and different initial preoscillation conditions of elasticity and glottal aperture are assessed given previous studies showing the coexistence of different vibration patterns related to voicing and voice register transitions [25].

In the following, first, the experimentally studied FS instability is described (Sec. II), and the sought correlation dimension $D_2$ is introduced (Sec. III). Next, results are outlined in Sec. IV, discussed in Sec. V, and a conclusion is formulated in Sec. VI.

## II. FLUID-STRUCTURE INSTABILITY

Upstream pressure signal $P_u(t)$ is measured during auto-oscillation of a deformable self-oscillating replica subjected to water spraying as detailed in Ref. [13]. Briefly, a uniform circular channel (diameter 2.5 cm) is mounted upstream (trachea, 12 cm) and downstream (vocal tract, 11 cm) from a deformable VF mechanical replica as shown in Fig. 1. The upstream channel is equipped with a pressure tap so that upstream pressure $P_u(t)$ can be measured with a pressure transducer (Endevco 8507C-5, accuracy $\pm 5$ Pa). The upstream channel is mounted to a pressure reservoir (volume $\geqslant 0.22$ m$^3$), conditioned to suppress parasite acoustic resonances, which is connected to a valve (Norgren, 11-818-987) controlled air supply (air compressor Altas Copco GA5 FF-300-8) [12].

*annemie.vanhirtum@univ-grenoble-alpes.fr

 

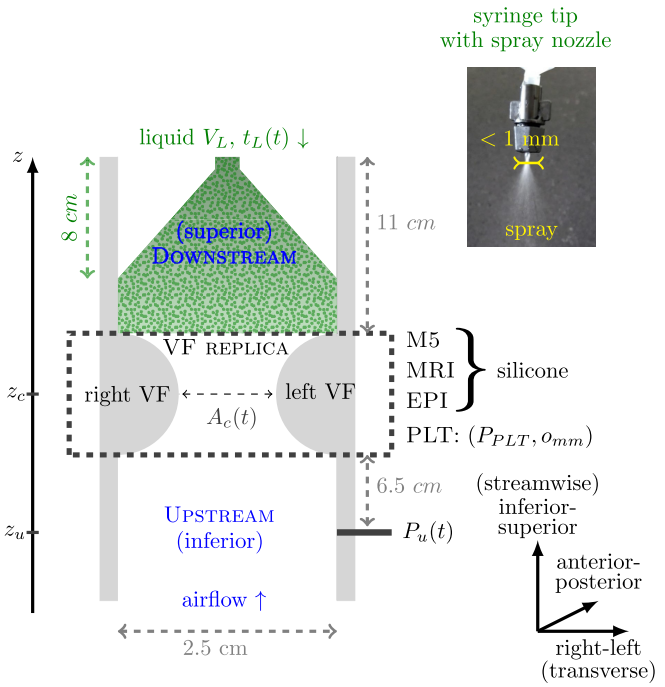


FIG. 1. Frontal view of experimental setup with measured liquid injection time-tag $t_L$, sprayed liquid volume $V_L$, and upstream pressure $P_u(t)$. Minimum area variation $A_c(t)$ is due to a FS interaction using a deformable VF replica.

During experiments, continuous steady airflow (density $\rho_G = 1.2\ \mathrm{kg\,m^{-3}}$, dynamic viscosity $\mu_G = 1.8 \times 10^{-5}$ Pa s, and temperature $22 \pm 2\,^{\circ}\mathrm{C}$) is provided so that the FS interaction between the airflow and the deformable VF replica results in a steady oscillatory pattern in the absence of water. Experiments are performed with mean upstream pressure $\bar{P}_u$ just above the minimum pressure associated with the subcritical Hopf bifurcation to sustain oscillation [26–28]. Then, distilled water (density $\rho_L = 998\ \mathrm{kg\,m^{-3}}$, dynamic viscosity $\mu_L = 1.0 \times 10^{-3}$ Pa s, and temperature $22 \pm 2\,^{\circ}\mathrm{C}$) is injected manually at the downstream end of the channel by emptying a graduated (accuracy 0.1 ml) syringe equipped with a spray nozzle (diffusion angle $20^{\circ} \pm 1^{\circ}$, diameter 1 mm) containing a known volume $V_L \leqslant 5$ ml. Water is sprayed homogeneously across the constricted area (Fig. 1). Water injection is time-tagged $t_L$ by manually operating an electrical switch at the start and end of each injection. Liquid injection duration takes less than 3 s for all $V_L$'s so that the overall order of the magnitude of liquid supply volume flow rate during injection yields $1.8 \pm 0.6$ ml/s [12]. It follows that the volume fraction during an oscillation cycle varies between zero during the closed phase up to 1 during the open phase [12]. The 5 s portions of upstream pressure $P_u(t)$ gathered 5 s after water injection finished are analyzed. This way, the impact of surface hydration with a spray is mimicked. All signals are acquired with sampling frequency $f_s = 10$ kHz corresponding to a temporal accuracy of 0.1 ms which yields $\leqslant$1.5% of the period for a signal with oscillation frequency $\leqslant$150 Hz.

The FS interaction is studied for different deformable VF replicas depicted in Fig. 2: pressurized latex tube (PLT detailed in Refs. [29–31]), VF replica, and deformable silicone VF replicas (labelled M5, MRI and EPI) molded as detailed in Refs. [13,32–35]).

The PLT VF replica (Fig. 2(a) [29–31]) consists of two latex tubes mounted in a metallic holder. Each VF latex tube (diameter 11 mm and thickness 0.2 mm) is pressurized ($P_{\mathrm{PLT}}$) by connecting it to a water column whose height can be changed so that the elasticity is determined by the internal pressure $P_{\mathrm{PLT}}$ of each latex tube. The position of each VF with respect to the centerline of the attached downstream and upstream tube (Fig. 1), and hence, the initial spacing between both VFs in the absence of airflow can then further be varied using micrometer screws (Mitutoyo 153-101, accuracy 0.01 mm, range 5 mm). Different $P_{\mathrm{PLT}}$ and screw openings $o_{mm}$ are assessed so that the initial glottal area ranges from 18 mm$^2$ up to 74 mm$^2$. Different initial PLT conditions are denoted as $(P_{\mathrm{PLT}}, o_{mm})$. Concretely, five different PLT VF replica conditions are considered—(2300,0), (2800,0), (3300,0), (2800,1), and (2800,2)—so that either $o_{mm}$ or $P_{\mathrm{PLT}}$ is deflected from condition (2800,0). Mean upstream pressure $\bar{P}_u$ yielded $250 < \bar{P}_u < 480$ Pa for the PLT VF replica conditions.

Deformable silicone VF replicas (Fig. 2(b) [13,32–35]) are molded so that their elasticity and initial apertures are constant. Three silicone VF replicas (M5, MRI, and EPI detailed in Refs. [13,32–35]) are considered which differ in geometry and composition, i.e., two (M5), three (MRI), or four (EPI) molding layers and a backing layer attaching it to a rigid support, i.e., region outside of the top view frames shown in Fig. 2(b). The M5 VF replica is a two-layer (muscle and

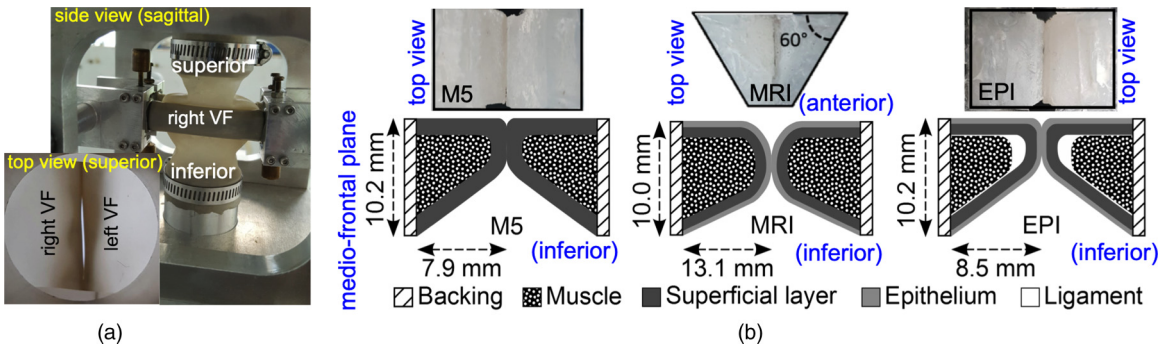


FIG. 2. Deformable mechanical VF replicas: (a) PLT with initial conditions $(P_{\mathrm{PLT}}, o_{mm})$ [29–31], (b) silicone moldings M5, MRI, and EPI [13,32–34].

superficial layer) reference model following the so called M5 geometrical VF model [36]. The MRI VF replica has a more realistic geometry derived from magnetic resonance imaging data of a human VF [34,35]. It has a three-layer structure by adding a third thin and stiff surface layer representing the epithelium to the two-layer structure of the M5 VF replica. The EPI VF replica is obtained by inserting an extremely soft deep layer between the muscle and the superficial layer of the three-layer structure used for the MRI VF replica [33]. The EPI VF replica cast is inspired on the geometrical M5 VF model so that its geometry is a scaled version of the M5 VF replica. The initial glottal area, i.e., spacing between VF without airflow, yields less than 10 $mm^2$ for all silicone VF replicas. Mean upstream pressure $\bar{P}_u$ yielded $\bar{P}_u \approx 460$ Pa for the EPI VF replica and $1450 < \bar{P}_u < 1800$ Pa for the MRI and M5 VF replicas.

## III. TIME SERIES ANALYSIS

The correlation dimension $D_2$ relies on a phase space reconstruction of the system dynamics from a series of measurements at equally spaced intervals in time [37]. Let $P_u(n)$ with $n = 1, \ldots, N$ denote the measured upstream pressure time series of length $N$. A set of $m$-dimensional reconstructed vectors $\mathbf{y}_i^m$ is generated using the method of delays as

$$\mathbf{y}_i^m = \{P_u(i), P_u(i+\tau), P_u(i+2\tau), \ldots, P_u[i+(m-1)\tau]\}^T, \tag{1}$$

where $\cdot^T$ is the transpose operator, $\tau$ indicates the time delay between consecutive samples in the reconstructed space, and $m$ denotes the embedding dimension so that $N_m = N - \tau(m-1)$ vectors can be reconstructed for each $m$ dimension [14,37,38]. The distance $d_{i,j}^m = d(\mathbf{y}_i^m, \mathbf{y}_j^m)$ between each pair of reconstructed vectors is computed as the Euclidean $l_2$ norm of the difference vector $\Delta\mathbf{y}_{i,j}^m = \mathbf{y}_i^m - \mathbf{y}_j^m$ so that

$$d_{i,j}^m = \sqrt{\sum_{k=1}^{m} \left[\mathbf{y}_i^m(k) - \mathbf{y}_j^m(k)\right]^2}. \tag{2}$$

The probability of the reconstructed vector pair distance being smaller than a certain threshold $r$ is then given by correlation sum $C_m(r)$,

$$C_m(r) = \frac{1}{N_m(N_m-1)} \sum_{\substack{i,\,j=1 \\ i \neq j}}^{N_m} H\left(r - d_{i,j}^m\right), \tag{3}$$

where $H(\cdot)$ indicates the Heaviside function so that $H(x) = 1$ for $x \geqslant 0$ and $H(x) = 0$ for $x < 0$. For large enough values of $r$, $d_{i,j} < r$ holds $\forall\{i, j\}$ combinations so that $C_m(r) = 1$. It follows that for deterministic systems $C_m(r)$ decreases monotonically from 1 towards 0 as $r$ approaches 0. Therefore, assuming $C_m(r) \approx r^{D_2^m}$ results in correlation dimension,

$$D_2^m = \lim_{r \to 0} \frac{\ln C_m(r)}{\ln r}. \tag{4}$$

The slope in the linear region of the $\ln C_m(r)$ versus $\ln r$ domain is considered as an estimation of $D_2^m$ [37,39–41]. For increasing embedding dimension $m$, $D_2^m$ converges to a finite value of $D_2$. As the system is more complex, i.e., as more degrees of freedom are required to describe the system's dynamics, $D_2$ is larger.

Time-delay $\tau$ is estimated as the first local minimum of the mutual information [37,40], and the required minimal embedding dimension $m$ is obtained using the method of false nearest neighbors [37,42,43]. Correlation dimension $D_2$ is then estimated from a recurrence analysis of the $N_m$ reconstructed phase space trajectories of upstream pressure $P_u$ [37,41,44]. The recurrence analysis is based on recurrence plots $R_{i,j}$ defined by the summation terms in Eq. (3) as

$$R_{i,j} = H\left(r - d_{i,j}^m\right). \tag{5}$$

Recurrence plots $R_{i,j}$ represent the number and duration of recurrent states and, as such, express the degree of predictability inherent to the system. For a fully predictable, i.e., deterministic, oscillating system states are recurrent as initially neighboring states remain so over time, and $R_{i,j}$ is characterized by uninterrupted diagonal lines. As chaos is introduced in the system, initially neighboring states will eventually diverge in time when the system loses its predictability so that $R_{i,j}$ is characterized by diagonal lines of finite length $l$. The shorter $l$ the faster states diverge and the more the system approaches a chaotic regime. Recurrence plots $R_{i,j}$ are then quantified considering the degree of determinism $\mathcal{D}$, the recurrence rate of states $\mathcal{R}$ and their ratio $\gamma = \mathcal{D}/\mathcal{R}$ defined as

$$\mathcal{D} = \frac{\sum_{l=l_{\min}}^{N_m} l\mathcal{P}(l)}{\sum_{l=1}^{N} l\mathcal{P}(l)}, \tag{6}$$

$$\mathcal{R} = \frac{1}{N_m^2} \sum_{i,\,j=1}^{N_m} R_{i,j}, \tag{7}$$

$$\gamma = N_m^2 \frac{\sum_{l=l_{\min}}^{N_m} l\mathcal{P}(l)}{\left(\sum_{l=1}^{N_m} l\mathcal{P}(l)\right)^2}, \tag{8}$$

with $\mathcal{P}(l)$ as the histogram of diagonal lines with lengths $l$ and minimum line length $l_{\min} \geqslant 2$. In addition, entropy $E$ is obtained from the probability distribution of the diagonal line lengths $p(l)$ as

$$E = -\sum_{l=l_{\min}}^{N_m} p(l) \ln_2 p(l). \tag{9}$$

## IV. RESULTS

Measured time series of upstream pressure $P_u(t)$ (left) and their phase representation (right) following water spraying with volumes $V_L \leqslant 5$ mL are illustrated in Fig. 3 for a silicone VF replica (MRI in Fig. 3(a)) and a PLT VF replica condition [(2800,0) in Fig. 3(b)]. To facilitate comparison between times series, $P_u$ is upshifted (+1500 Pa) with each $V_L$ increment, and time $t$ is normalized with respect to the lowest characteristic oscillation period $1/f_N$ with $f_N(V_L)$ as indicated for each time trace. For all VF replicas, embedding dimension $m$ varies in the range of $10 \leqslant m \leqslant 25$, and time-delay $\tau$ varies in the range of $15 \leqslant \tau \leqslant 35$. Water spraying enhances auto-oscillation for all VF replicas since the lowest characteristic oscillation frequency $f_N$ decreases with $V_L$ and from the phase space trajectories is seen that the

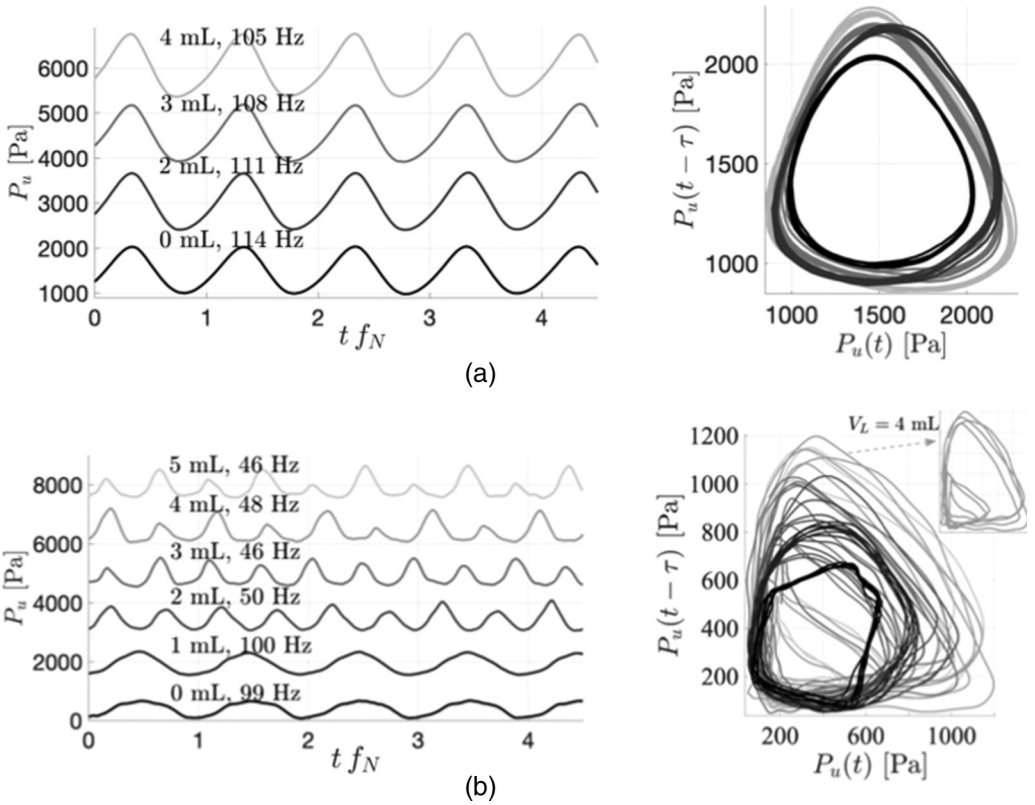


FIG. 3. Illustration of upstream pressure time series $P_u(t\,f_N)$ (left) and their phase space representation (right) for volumes $V_L \leqslant 5$ ml (gray scaling indicating $V_L$ in milliliters and $f_N$ in hertz) for (a) silicone (MRI) and (b) PLT [condition (2800,0)] VF replicas. For clarity, time series $P_u(t\,f_N)$ are upshifted (+1500 Pa) with each $V_L$ increment.

oscillation amplitude increases which confirms findings reported in Ref. [13]. For silicone VF replicas, $f_N$ corresponds to the first harmonic, whereas for PLT VF replica conditions, a subharmonic frequency is generated as observed from the period doubling for $V_L \geqslant 2$ ml in Fig. 3(b). As a consequence, the phase state representation for the silicone VF replicas exhibits a single oscillation trajectory regardless of $V_L$ associated with a stable deterministic oscillation regime for each $V_L$. For PLT VF replica conditions, the generation of a subharmonic oscillation frequency makes the phase trajectory more complicated as single oscillation cycles [$V_L \in \{2, 3\}$ ml in Fig. 3(b)] become less stable until [$V_L \in \{4, 5\}$ in Fig. 3(b)] an inner cycle imprints on the trajectory due to the growth of the subharmonic with $V_L$ so that the trajectory in phase space approaches a chaotic oscillatory regime as divergences of the cycles in phase space can be observed as $V_L$ increases.

Recurrence plots [Eq. (5)] of the phase space state trajectories are illustrated in Fig. 4 for $V_L \in \{2, 4\}$ ml for the silicone (MRI) and PLT VF replica [condition (2800,0)]. For $V_L = 2$ ml, both recurrence plots display a regular pattern of diagonal lines reflecting the harmonic properties of the auto-oscillation. For $V_L = 2$ ml, recurrence plots can reveal some degree of loss of determinism illustrated for the PLT VF replica at $V_L = 4$ ml [Fig. 4(d)] as irregular shorter diagonal lines are observed. The MRI replica, on the other hand, remains in a deterministic oscillatory regime for $V_L = 4$ ml [Fig. 4(c)].

Recurrence plot properties [$\mathcal{D}$, $\mathcal{R}$, and $\gamma$ defined in Eq. (8)] are then quantified for all VF replicas as a function of $V_L$. Degree of determinism $\mathcal{D}(V_L)$, recurrence rate $\mathcal{R}(V_L)$, and their ratio $\gamma(V_L)$ are plotted in Fig. 5. For $V_L = 2$ ml, all VF replicas exhibit a stable oscillatory pattern as $\mathcal{D} > 90\%$ in Fig. 5(a), i.e., recurrence plot with mostly uninterrupted diagonal lines as shown in Figs. 4(a) and 4(b). As $V_L$ increases, silicone VF replicas remain characterized by a stable deterministic pattern [e.g., Fig. 4(c)] so that $\mathcal{D} > 90\%$ for all $V_L$'s. PLT VF replica conditions, on the other hand, approach chaotic behavior as $V_L$ increases so that $\mathcal{D}$ reduces to within the range of $70\% < \mathcal{D} < 90\%$ for $V_L \in \{4, 5\}$ ml. Recurrence rates $\mathcal{R}(V_L)$ [Fig. 5(b)] and ratios $\gamma(V_L)$ [Fig. 5(c)] further confirm tendencies described for $\mathcal{D}$. Recurrence rate $\mathcal{R}$ increases as a system approaches a chaotic regime as more states occur compared to the stable deterministic regime. The increase in $\mathcal{R}$ remains negligible ($\leqslant 2\%$) for silicone VF replicas regardless of $V_L$ whereas it increases with up to 10% for PLT VF replicas for $V_L = 2$ ml. It follows that ratio $\gamma$ is maximum (high $\mathcal{D}$ and low $\mathcal{R}$) for $V_L \in \{0, 1\}$ ml since the auto-oscillation result in a deterministic stable oscillation for all VF replicas. For $V_L = 2$ ml, $\gamma$ will decrease with a degree and at a rate proper to each VF replica and imposed initial conditions ($P_{\mathrm{PLT}}$, $o_{mm}$). The decrease remains limited to $<20\%$ for silicone VF replicas ($6.1 \geqslant \gamma \geqslant 5.1$) indicating a deterministic oscillation regime and becomes significant up to $<50\%$ ($5.7 \geqslant \gamma \geqslant 2.8$) for some PLT VF replica initial ($P_{\mathrm{PLT}}$, $o_{mm}$) conditions indicating the loss of stable oscillation.

Quantified properties $\mathcal{D}(V_L)$, $\mathcal{R}(V_L)$, and their ratio $\gamma(V_L)$ suggest that water spraying ($V_L > 0$ ml) can cause the oscillation pattern to approach a chaotic complex oscillation pattern

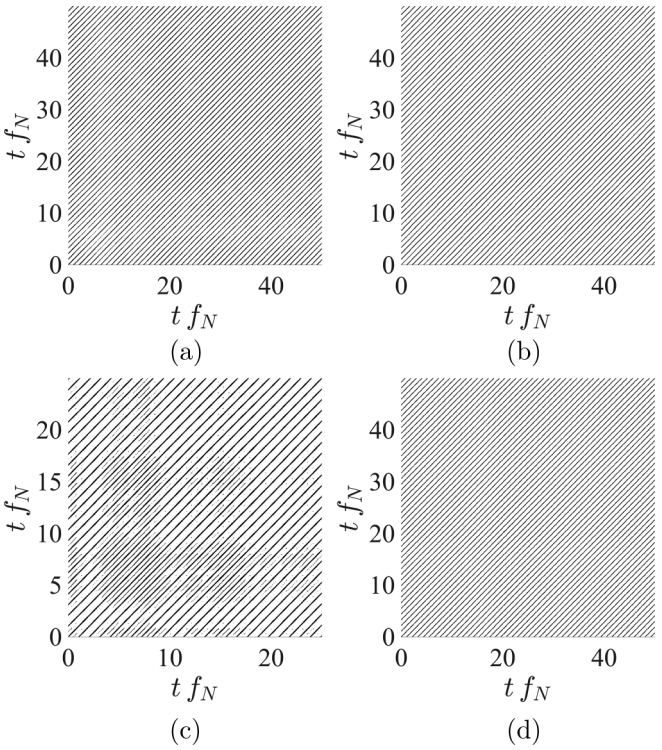


FIG. 4. Recurrence plots for $V_L \in \{2, 4\}$ ml for VF replicas PLT condition (2800,0) and silicone MRI: (a) PLT with $V_L = 2$ ml, (b) MRI with $V_L = 2$ ml, (c) PLT with $V_L = 4$ ml, and (d) MRI with $V_L = 4$ ml.

depending on the VF replica, imposed initial conditions, and on $V_L$. The complexity of the auto-oscillation is quantified by entropy $E(V_L)$ [Eq. (9)] and estimated correlation dimension $D_2(V_L)$ [Eq. (4)] plotted in Fig. 6. Overall entropy $E(V_L)$ [Fig. 6(a)] shows a small increase in the range of $7.7 \leqslant E(V_L) \leqslant 9.0$ for PLT VF replica conditions whereas it remains of similar magnitude for the silicone VF replicas within the range of $7.5 \leqslant E(V_L) \leqslant 8.6$. Nevertheless, $E(V_L)$ tendencies are not sufficiently pronounced to sustain a conclusion. Correlation dimension estimates $D_2(V_L)$ are shown in Fig. 6(b). For $V_L < 2$ ml, $1.01 < D_2 < 1.12$ holds and increases for $V_L \geqslant 2$ ml at a rate which differs between VF replicas. For silicone VF replicas, the increase is limited to within 10% as $1.01 < D_2(V_L) < 1.12$. For PLT VF replica conditions, the increase is more pronounced and yields up to 85% as $1.07 < D_2(V_L) < 2.00$ holds.

## V. DISCUSSION

The phase space state and recurrence plot analysis, presented in Sec. IV, shows that estimated correlation dimension $\mathcal{D}_2$ (increase within 85%) and ratio $\gamma$ (decrease within 50%) are suitable quantities to express changes to the complexity of the steady state auto-oscillation pattern due to surface hydration following water spraying.

Observed $\gamma(V_L)$ and $D_2(V_L)$ tendencies indicate that water spraying for $V_L \leqslant 5$ ml does not impact the deterministic oscillation regime for silicone VF replicas whereas the system approaches a chaotic regime for PLT VF replica conditions.

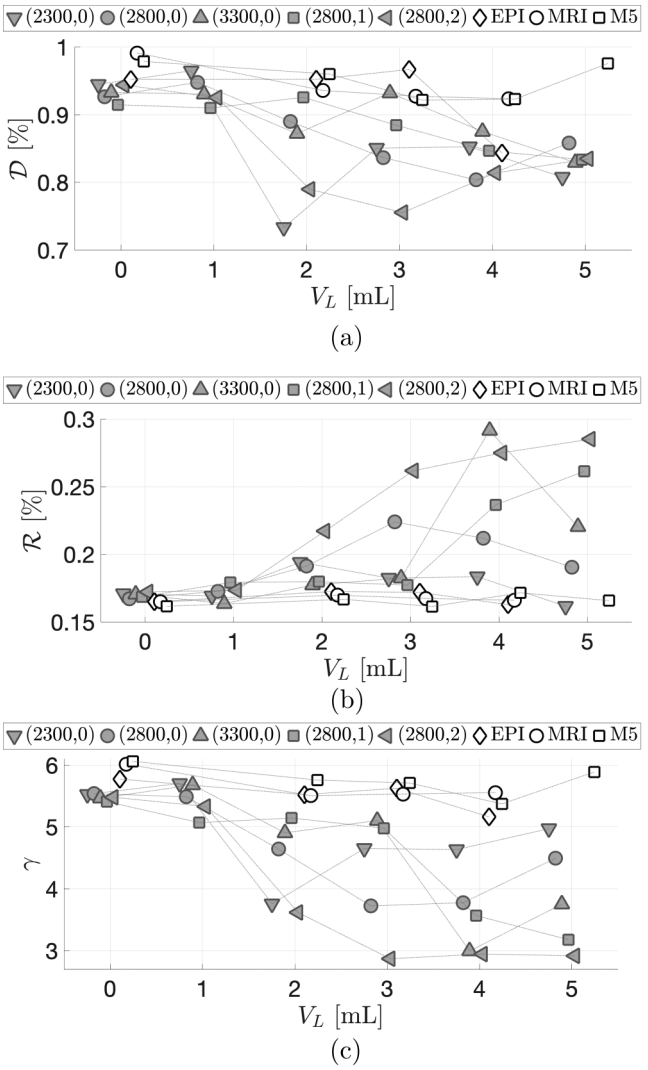


FIG. 5. (a) Degree of determinism $\mathcal{D}(V_L)$, (b) recurrence rate $\mathcal{R}(V_L)$, and (c) their ratio $\gamma(V_L)$ for VF replicas (symbols) shifted around each $V_L$ value for clarity.

This confirms observations reported for the signal-to-noise ratio and the fast cycle-to-cycle perturbations of amplitude and period [13]. The increased overall stability of the auto-oscillation for silicone VF replicas compared to PLT VF replicas is in line with the initial complexity observed for $V_L = 0$ ml as $\gamma(V_L = 0)$ and $D_2(V_L = 0)$ are larger and lower, respectively, for silicone VF replicas than for PLT replica conditions.

For the PLT replica and $V_L \in \{0, 1\}$ ml recurrence, plots exhibit a pattern of diagonal lines so that $D_2$ is near unity and $\gamma$ is near its maximum, which is inherent to a deterministic oscillation pattern. For $V_L \geqslant 2$ ml, the oscillation regime becomes more complicated as period doubling is observed, the degree of determinism $\mathcal{D}$ decreases, and the recurrence rate $\mathcal{R}$ increases illustrating that the system loses some of its predictability as chaos is introduced in the system. The degree to which the initial stable oscillation pattern is disturbed depends on the imposed initial conditions of aperture ($o_{mm} \in \{0–2\}$ and $P_{\mathrm{PLT}} = 2800$) and elasticity ($P_{\mathrm{PLT}} \in \{2300, 2800, 3300\}$ and

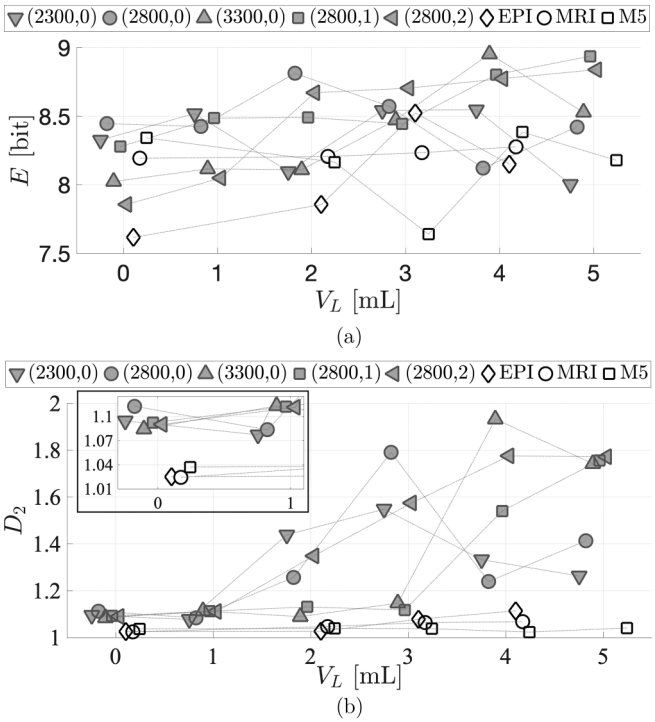


FIG. 6. (a) Entropy $E(V_L)$ and (b) estimated correlation dimension $D_2(V_L)$ for VF replicas (symbols) shifted around each $V_L$ value for clarity. The frame contains a zoom for $D_2(V_L)$ with $V_L \in \{1, 2\}$ ml.

$o_{mm} = 0$). Estimated $\mathcal{D}_2$ and $\gamma$ tendencies suggest that the complexity increases with initial aperture (increase of $o_{mm}$) and with rigidity (increase of $P_{\mathrm{PLT}}$).

For future research, it is of interest to investigate the influence of initial conditions and the influence of the imposed $\bar{P}_u$ on the initial oscillation complexity for $V_L = 0$ ml and on the complexity increase following hydration by water spraying ($V_L > 0$ ml). This way the influence of initial conditions on the coexistence of different attractors can be further studied [25]. In particular, the role of aerodynamic turbulence needs further investigation, and direct observation of the oscillation might contribute to the understanding of the effect of hydration in terms of oscillation modes [45–47]. Spraying with other liquids needs to be assessed in order to increase the relevance with respect to VF surface hydration and artificial saliva sprays.

It is noted that the estimated range of $D_2(V_L)$ values ($1 \leqslant D_2 \leqslant 2$) observed for the mechanical VF replicas is similar to the range reported for human speakers during normal voicing by several researchers [15–19]. This encourages further quantification of $D_2$ as well as $\gamma$ in order to inform on the oscillation regime and its complexity.

## VI. CONCLUSION

The use of different mechanical VF replicas showed that after water is sprayed ($V_L \leqslant 5$ ml) on a stable auto-oscillation either the deterministic regime is maintained or the oscillation approaches a chaotic regime introduced by period doubling. Phase space state recurrence feature $\gamma$, i.e., the ratio of the degree of determinism to the recurrence rate of the phase space states, and estimated correlation dimension $D_2$ are suitable parameters to express the influence of hydration following water spraying on the oscillation regime. Besides initial pre-oscillatory conditions related to the glottal aperture and VF elasticity also the initial FS complexity determine the impact of water spraying on the complexity of the oscillation regime. The initial complexity near the onset pressure of oscillation is found to be lower for silicone VF replicas than for PLT VF replica conditions. Future research perspectives are outlined.

## ACKNOWLEDGMENTS

This work was partly supported by ArtSpeech Project (Project No. ANR-15-CE23-0024). The authors are grateful to Dr. I. Tokuda (Ritsumeikan University, Japan) for providing silicone VF casts.

[1] K. Verdolini, I. R. Titze, and A. Fernell, Dependence of phonatory effort on hydration level, J. Speech Hear Res **37**, 1001 (1994).

[2] K. Verdolini, M. Sandage, and I. R. Titze, Effect of hydration treatments on laryngeal nodules and polyps and related voice measures, J. Voice **8**, 30 (1994).

[3] N. Roy, K. Tanner, S. D. Gray, M. Blomgren, and K. V. Fisher, An evaluation of the effects of three laryngeal lubricants on phonation threshold pressure (PTP), J. Voice **17**, 331 (2003).

[4] C. Leydon, M. Sivasankar, D. L. Falciglia, C. Atkins, and K. Fisher, Vocal fold surface hydration: a review, J. Voice **23**, 658 (2009).

[5] C. Leydon, M. Wroblewski, N. Eichorn, and M. Sivasankar, A meta-analysis of outcomes of hydration intervention on phonation threshold pressure, J. Voice **24**, 637 (2010).

[6] M. Alves, E. Kruger, B. Pillay, K. van Lierde, and J. van der Linde, The effect of hydration on voice quality in adults: a systematic review, J. Voice **33**, 13 (2019).

[7] N. Ruty, X. Pelorson, A. Van Hirtum, I. Lopez, and A. Hirschberg, An in-vitro setup to test the relevance and the accuracy of low-order models of the vocal folds, J. Acous. Soc. Am. **121**, 479 (2007).

[8] B. Fabre, J. Gilbert, A. Hirschberg, and X. Pelorson, Aeroacoustics of musical instruments, Annu. Rev. Fluid. Mech. **44**, 1 (2012).

[9] R. Mittal, B. D. Erath, and M. W. Plesniak, Fluid dynamics of human phonation and speech, Annu. Rev. Fluid. Mech. **45**, 437 (2013).

[10] Y. Zhang, J. J. Jiang, and S. M. Wallace, Comparison of nonlinear dynamic methods and perturbation methods for voice analysis, J. Acous. Soc. Am. **118**, 2551 (2005).

[11] K. Tanner, N. Roy, R. M. Merrill, K. Kendall, K. L. Miller, D. O. Clegg, A. Heller, D. R. Houtz, and M. Elstad, Comparing nebulized water versus saline after laryngeal desiccation challenge in Sjögren's Syndrome, Laryngoscope **123**, 2787 (2013).

[12] A. Van Hirtum, A. Bouvet, and X. Pelorson, Pressure drop for adiabatic air-water flow through a time-varying constriction, Phys. Fluids **30**, 101901 (2018).

[13] A. Bouvet, X. Pelorson, and A. Van Hirtum, Influence of water spraying on an auto-oscillating channel (unpublished).

[14] F. Takens, *Dynamical Systems and Turbulence* (Springer-Verlag, Berlin, 1981), pp. 1–366.

[15] J. Jiang, Y. Zhang, and C. McGiligan, Chaos in voice, from modeling to measurement, J. Voice **20**, 2 (2006).

[16] S. N. Awan, N. Roy, and J. J. Jiang, Nonlinear dynamic analysis of disordered voice: the relationship between the correlation dimension (D2) and pre-/post treatment change in perceived dysphonia severity, J. Voice **25**, 285 (2010).

[17] S. H. Choi, Y. Zhang, J. J. Jiang, D. M. Bless, and N. V. Welham, Nonlinear dynamic-based analysis of severe dysponia in patients with vocal fold scar and sulcus vocalis, J. Voice **26**, 566 (2012).

[18] L. Lin, Y. Zhang, W. Calawerts, and J. J. Jiang, Vibratory dynamics of four types of excised larynx phonations, J. Voice **30**, 649 (2016).

[19] B. Liu, E. Polce, J. C. Sprott, and J. J. Jiang, Applied chaos level test for validation of signal conditions underlying optimal performance of voice classification methods, J. Speech Lang Hear Res. **61**, 1130 (2018).

[20] W. Mende, H. Herzel, and K. Wermke, Bifurcations and chaos in newborn infant cries, Phys. Lett. A **145**, 418 (1990).

[21] H. Herzel and J. Wendler, *EUROSPEECH '91, Second European Conference on Speech Communication and Technology, Genova, Italy, 1991* (ISCA, Baixas, France 1991), pp. 263–266.

[22] M. Banbrook, S. McLaughlin, and I. Mann, Speech characterization and synthesis by nonlinear methods, IEEE Trans. Speech Audio Proc. **7**, 1 (1999).

[23] A. Behrman, Global and local dimensions of vocal dynamics, J. Acous. Soc. Am. **105**, 432 (1999).

[24] P. Maragos and A. Potamianos, Fractal dimensions of speech sounds: computation and application to automatic speech recognition, J. Acous. Soc. Am. **105**, 1925 (1999).

[25] I. T. Tokuda, J. Horacek, J. G. Svec, and H. Herzel, Comparison of biomechanical modeling of register transitions and voice instabilities with excised larynx experiments, J. Acoust. Soc. Am. **122**, 519 (2007).

[26] D. A. Berry, H. Herzel, I. R. Titze, and B. H. Story, Bifurcations in excised larynx experiments, J. Voice **10**, 129 (1996).

[27] P. Mergell, H. Herzel, T. Wittenberg, M. Tigges and U. Eysholdt, Phonation onset: vocal fold modeling and high-speed glottography, J. Acoust. Soc. Am. **104**, 464 (1998).

[28] J. C. Lucero, A theoretical study of the hysteresis phenomenon at vocal fold oscillation onset-offset, J. Acous. Soc. Am. **105**, 423 (1999).

[29] J. Haas, P. Luizard, X. Pelorson, and J. Lucero, Study of the effect of a moderate asymmetry on a replica of the vocal folds, Acta Acust. Acust. **102**, 230 (1987).

[30] P. Luizard and X. Pelorson, Threshold of oscillation of a vocal folds replica with unilateral surface growths, J. Acous. Soc. Am. **141**, 3050 (2017).

[31] A. Van Hirtum and X. Pelorson, High-speed imaging to study an auto-oscillating vocal fold replica for different initial conditions, Int. J. Appl. Mech. **9**, 1750064 (2017).

[32] P. R. Murray and S. L. Thomson, Synthetic, multi-layer, self-oscillating vocal fold model fabrication, J. Vis. Exp. **58**, e3498 (2011).

[33] P. R. Murray and S. L. Thomson, Vibratory responses of synthetic, self-oscillating vocal fold models, J. Acous. Soc. Am. **132**, 3428 (2012).

[34] I. T. Tokuda and R. Shimamura, Effect of level difference between left and right vocal folds on phonation: Physical experiment and theoretical study, J. Acous. Soc. Am. **142**, 482 (2017).

[35] B. A. Pickup and S. L. Thomson, Flow-induced vibratory response of idealized versus magnetic resonance imaging-based synthetic vocal fold models, J. Acous. Soc. Am. **128**, 124 (2010).

[36] R. Scherer, D. Shinwari, K. D. De Witt, C. Zhang, B. Kucinschi, and A. Afjeh, Intraglottal pressure profiles for a symmetric and oblique glottis with a divergence angle of 10 degrees, J. Acous. Soc. Am. **109**, 1616 (2001).

[37] H. Kantz and T. Schreiber, *Nonlinear Time Series Analysis* (Cambridge University Press, Cambridge, UK, 2003).

[38] J. C. Robinson, A topological delay embedding theorem for infinite-dimensional dynamical systems, Nonlinearity **18**, 2135 (2005).

[39] P. Grassberger and I. Procaccia, Characterization of Strange Attractors, Phys. Rev. Lett. **50**, 346 (1983).

[40] A. M. Fraser and H. L. Swinney, Independent coordinates for strange attractors from mutual information, Phys. Rev. A **33**, 1134 (1986).

[41] J. A. Lee and M. Verleysen, *Nonlinear Dimensionality Reduction* (Springer, Berlin, 2007), p. 308.

[42] M. B. Kennel, R. Brown, and H. D. I. Abarbanel, Determining embedding dimension for phase-space reconstruction using a geometrical construction, Phys. Rev. A **45**, 3403 (1992).

[43] R. Hegger and H. Kantz, Improved false nearest neighbor method to detect determinism in time series data, Phys. Rev. E **60**, 4970 (1999).

[44] J. P. Eckmann, S. O. Kamphorst, and D. Ruelle, Recurrence plots of dynamical systems, Europhys. Lett. **4**, 973 (1987).

[45] J. Neubauer, P. Mergell, U. Eysholdt, and H. Herzel, Spatio-temporal analysis of irregular vocal fold oscillations: biphonation due to desynchronization of spatial modes, J. Acoust. Soc. Am. **110**, 3179 (2001).

[46] P. Mergell, H. Herzel, and I. R. Titze, Irregular vocal-fold vibration. High-speed observation and modelling, J. Acoust. Soc. Am. **108**, 2996 (2000).

[47] I. Steinecke, and H. Herzel, Bifurcations in an symmetric vocal-fold model, J. Acoust. Soc. Am. **97**, 1874 (1995).